

## Wideband Optical Networks [WON]

Grant agreement ID: 814276

### WP2 – Digital signal processing and system modelling

#### Deliverable D2.4 Nonlinear impairment monitoring techniques and algorithms



*This project has received funding from the European Union's Horizon 2020 research and innovation programme under the Marie Skłodowska-Curie grant agreement 814276.*

## Document Details

Work Package	WP2 – Digital signal processing and system modelling
Deliverable number	D2.4
Deliverable Title	Nonlinear impairment monitoring techniques and algorithms
Lead Beneficiary:	POLITO
Deliverable due date:	31 July 2022
Actual delivery date:	7 November 2022
Dissemination level:	Public

## Project Details

Project Acronym	WON
Project Title	Wideband Optical Networks
Call Identifier	H2020-MSCA-2018 Innovative Training Networks
Coordinated by	Aston University, UK
Start of the Project	1 January 2019
Project Duration	48 months
WON website:	<a href="https://won.astonphotonics.uk/">https://won.astonphotonics.uk/</a>
CORDIS Link	<a href="https://cordis.europa.eu/project/rcn/218205/en">https://cordis.europa.eu/project/rcn/218205/en</a>

## WON Consortium and Acronyms

Consortium member	Legal Entity Short Name
Aston University	Aston
Danmarks Tekniske Universitet	DTU
VPIphotonics GmbH	VPI
Infinera Portugal	INF PT
Fraunhofer HHI	HHI
Politecnico di Torino	POLITO
Technische Universiteit Eindhoven	TUE
Universiteit Gent	UG
Keysight Technologies	Keysight
Finisar Germany GmH	Finisar
Orange SA	Orange
Technische Universitaet Berlin	TUB
Instituto Superior Tecnico, University of Lisboa	IST

**CONTENTS**

ABBREVIATIONS.....	4
LIST OF FIGURES .....	5
EXECUTIVE SUMMARY .....	6
1. Introduction.....	7
2. C+L single channel link tomography experimental setup, description and results .....	8
3. C+L multi-channel transmission link tomography experimental setup, description of denoising and results.....	10
4. Conclusions .....	13
5. REFERENCES .....	14

## ABBREVIATIONS

MBT:	Multi-band transmission
SMF:	Single-mode fiber
GA:	Grant Agreement
OPM:	Optical performance monitoring
PPE:	Power profile estimator
DSP:	Digital signal processing
EDFA:	Erbium-doped fiber amplifier
DAC:	Digital-to-analog converter
ECL:	External cavity lasers
CPR:	Carrier Phase Recovery
OLS:	Open line system
ILA:	Inline amplifiers
VOA:	Variable optical attenuator
RTO:	Real-time oscilloscope
CDC:	Chromatic dispersion compensator
DAE:	Data-aided equalizer
CPR:	Carrier phase recovery
FOC:	Frequency offset correction
OSA:	Optical spectrum analyser
WSS:	Wavelength selective switches
CUT:	Channel under test
BPF:	Bandpass filter
LO:	Local oscillator
DWT:	Discrete wavelet transformation

## LIST OF FIGURES

<b>Figure 1:</b> Experimental testbed and DSP scheme used in the link tomography. ....	8
<b>Figure 2:</b> Estimated spectral power profile for ILAs (a) 1, (c) 2 and (e) 3, and estimated gain spectrum, measurements, absolute error and mean error for ILA (b) 1, (d) 2 and (f) 3. ....	9
<b>Figure 3:</b> For a wavelength-dependent attenuator, (a) estimated gain spectrum of ILA 1, (b) Gain spectra of ILA 1 with and without emulated gain tilts, (c) Anomaly detection scheme, Anomaly indicator of (d) weak and (e) strong tilt. ....	9
<b>Figure 4:</b> Experimental testbed used in the multi-channel transmission link tomography. ....	10
<b>Figure 5:</b> (a) Link tomography obtained in Experiment II (multi-channel analysis). Power peak curves obtained from the link tomography obtained at (b) input of the OLS, and output of the ILA (c) 1, (d) 2 and (e) 3 link. ....	10
<b>Figure 6:</b> (a) Anomaly detection scheme based on subtraction. (b) Estimated anomaly heatmap for VOA with 6 dB of spectrally flat loss applied at the input of ILA 2. ....	11
<b>Figure 7:</b> Anomaly detection schemes based on (a) subtraction plus numerical differentiation, and (b) wavelet denoising. ....	11
<b>Figure 8:</b> Estimated anomaly heatmaps for subtraction plus numerical differentiation in (a) ILA 2 and (b) ILA 3, and for wavelet denoising in (c) ILA 2 and (d) ILA 3. (e) Comparison of anomaly detection curve in EDFA 2 in wavelength 1549 nm using subtraction plus numerical differentiation and wavelet denoising. ....	12

## EXECUTIVE SUMMARY

The present scientific deliverable is part of the Work Package 2 “Digital signal processing and system modelling”, of the ETN project WON “Wideband Optical Networks”, funded under the Horizon 2020 Marie Skłodowska-Curie scheme Grant Agreement 814276.

This document provides details on the state-of-art receiver-digital signal processing schemes used as a tool for fault detection in multi-band transmission systems, also being able to estimate the distance-wise and frequency-dependent channel power evolution. Consequently, this receiver can estimate the gain spectrum of each amplifier deployed in the optical line system, as well as soft failures in the amplifiers, such as gain tilts. Moreover, is presented two transmission scenarios: single channel transmission and a more realistic scenario, composed by a WDM transmission comb of 42 channels. It is also shown the application of a wavelet denoising anomaly detection, showing good improvement regarding accuracy.

## 1. Introduction

The deployment of multi-band transmission (MBT) [1] systems in optical networks has emerged as a cost-effective short/mid-term solution in order to cope with the recent growth in network traffic. This technology aims to increase the fiber bandwidth used in coherent transmission, from current value of 4.8 THz (in the C-band) up to approximately 40 THz in single-mode fibers (SMFs) within the low loss window. One aspect of the viability of this solution is due to the capability of optical performance monitoring (OPM) in transceivers. Recently, a variety of link properties extracted by the receiver-digital signal processing (Rx-DSP) are shown. As example, the longitudinal power evolution is shown in [2] and [3]. In [4] is evaluated the frequency response of bandpass filters and in [5] the span-wise chromatic dispersion mapping. The Raman gain is addressed in [6] and the polarization-dependent loss profile in [7]. Retrieving the link properties by the Rx-DSP enables the measurement of wavelength-dependent and spatially distributed physical characteristics of the optical networks in a cost-effective way [8]. This approach can remove the requirement of numerous in-line monitoring devices. In this context, this work shows the extension proposed in [3] of an *in-situ* power profile estimator (PPE) to work not only for distance-wise, but also in a wavelength-dependent way for a C+L line system of 280 km of SMF.

The results show that is possible to use this Rx-DSP link-tomography to estimate the gain spectrum of each erbium-doped fiber amplifier (EDFA) and to detect failures caused by amplifier gain tilt, all shown for single channel transmission. Moreover, this work also shows the link tomography results presented in [9] for a C+L wavelength division multiplexing (WDM) comb, approaching a more realistic optical network transmission scenario. Moreover, it introduces a denoising tool for anomaly detection, delivering a more uniform reading of the anomaly signatures.

## 2. C+L single channel link tomography experimental setup, description and results

The experimental testbed is shown on the upper part of Figure 1. The partially disaggregated line system is made of a transmitter, consisting of a 4-ch 84 GSa/s digital-to-analog converter (DAC) and a C-band optical multi-format transmitter. The wavelengths under test lie within the C- and L-bands, generated by two tunable external cavity lasers (ECLs). A 64-GBd DP 16-QAM signal is then generated with a  $2^{15}$  random bit sequence and shaped with a root-raised cosine pulse filter with a roll-off factor of 0.1. The optical line system (OLS) domain consists of 2 spans of 80 km and 2 spans of 60 km, with three inline amplifiers (ILAs) C+L EDFAs. It is worth noting that at the output of each ILA there is a variable optical attenuator (VOA) used to control the total input fiber power, with this value known *a priori*. At the receiver side, the signal is amplified by another C+L EDFA, before reaching the coherent receiver. Then, it is digitized by a 200 GS/s real-time oscilloscope (RTO). By tuning the ECLs in steps of 2.5 nm, it was able to emulate multiple WDM carriers within the C- and L-bands.

The link tomography scheme is shown on the bottom part of Figure 1. After the RTO, we blindly estimate and fully compensate the link-accumulated chromatic dispersion ( $c_{tot}$ ) by a chromatic dispersion compensator (CDC). Then, a data-aided equalizer (DAEQ) is used for polarization demultiplexing before being split into two tributaries, 1 and 2. Tributary 1 consists of a reloading  $c_{tot}$  module, partial CDC of  $n \times c_{tot}/N_{seg}$  (in which  $n$  is a integer number varying from 0 to  $N_{seg}$ , which is the total number of link segments), a nonlinear remediator (which compensates for nonlinear phase noise due to Kerr effect) and a residual CDC. Tributary 2 is based on a standard DSP chain to recover the signal, consisting of a carrier phase recovery (CPR) stage, frequency offset correction (FOC), and a decision based on the nearest complex symbol. The correlation between the tributaries produces the longitudinal power profile for each wavelength tested.

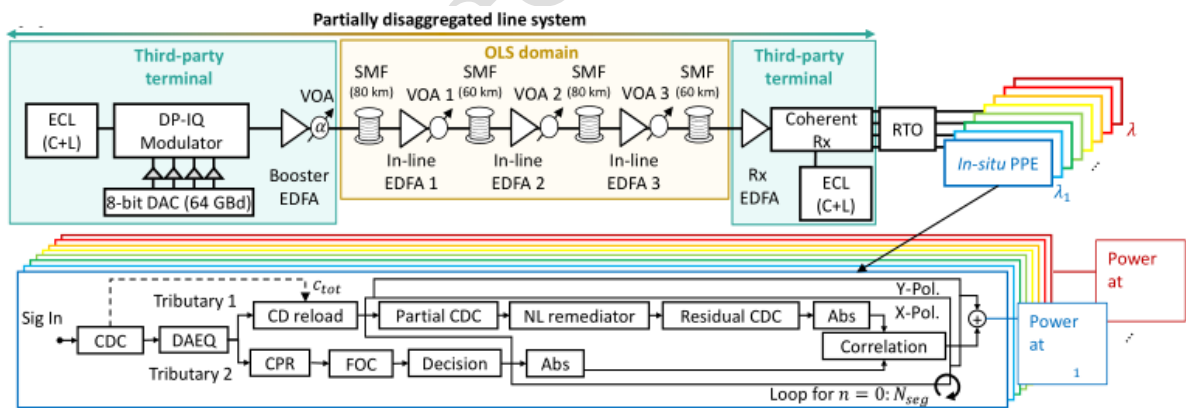


Figure 1: Experimental testbed and DSP scheme used in the link tomography.

Using the link tomography described above, we intend to estimate the gain spectra of ILAs 1, 2 and 3 (which here is a combination of amplifier gain plus VOA) and detect EDFA soft failures (in our case, of ILA 1), such as gain tilt.

The estimated spectral power profile is presented in Figure 2 (a), (c) and (e) for ILAs 1, 2 and 3, respectively. In Figure 2 (b), (d) and (f) the estimated gain profile (cross-like markers) is compared with the optical spectrum analyser (OSA) measurements (circle-like markers). The absolute and mean

error is also shown for each case. These results show good agreement, presenting mean errors (dashed line) of 0.4, 0.5 and 0.6 dB for ILAs 1, 2 and 3, respectively, showing that link tomography presents a reliable way to estimate the gain profile of all ILAs with good accuracy.

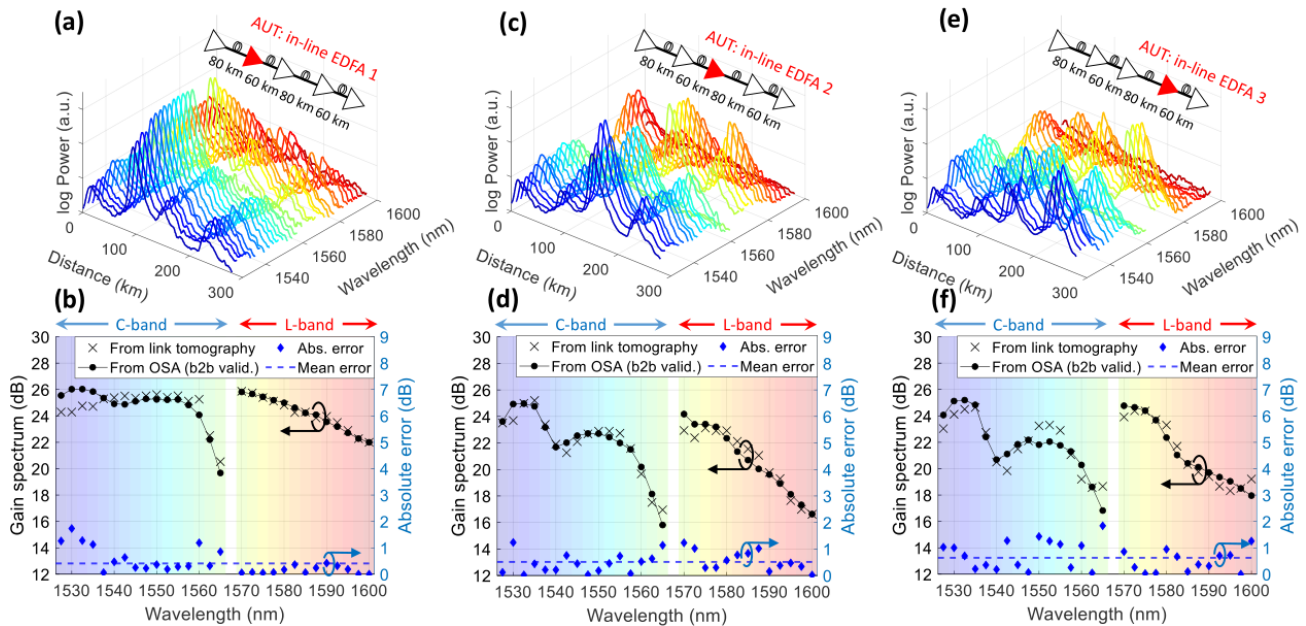


Figure 2: Estimated spectral power profile for ILAs (a) 1, (c) 2 and (e) 3, and estimated gain spectrum, measurements, absolute error and mean error for ILA (b) 1, (d) 2 and (f) 3.

In

Figure 3 (a) the estimated gain profile and measurements for ILA 1 are presented without intervening in the link. Next, gain tilt is emulated by setting a wavelength-dependent attenuator at the end of ILA 1. The two tilt profiles (weak and strong) are shown in Figure 3 (b) with its respective gain profile. The anomaly, which is a simple subtraction of the anomalous link tomography from the normal state link tomography (Figure 3 (c)), is shown in Figure 3 (d-e), showing a good fidelity of the two tested profiles, denoted by the gradual colouring of the heat map. It is also possible to see that the strong tilt (Figure 3 (e)) causes a strong cascade effect in ILAs 2 and 3, as these amplifiers can no longer maintain a constant output power. Again, these results indicate that the link tomography can detect EDFA failures without additional testing equipment or access to the infrastructure information.

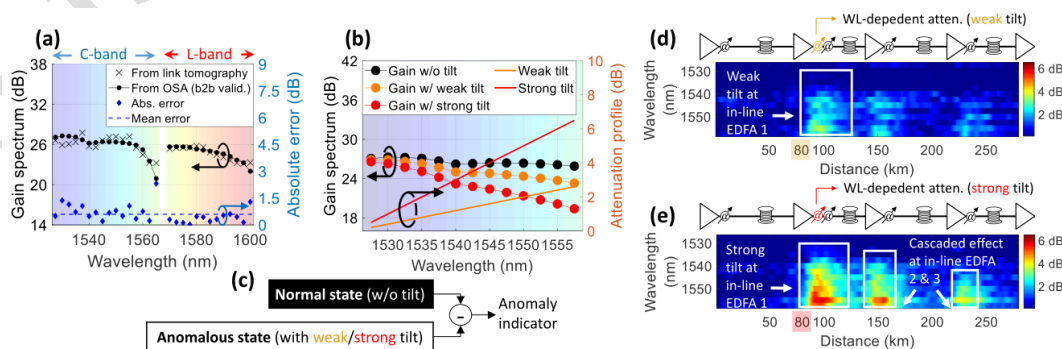


Figure 3: For a wavelength-dependent attenuator, (a) estimated gain spectrum of ILA 1, (b) Gain spectra of ILA 1 with and without emulated gain tilts, (c) Anomaly detection scheme, Anomaly indicator of (d) weak and (e) strong tilt.

### 3. C+L multi-channel transmission link tomography experimental setup, description of denoising and results

For the multi-channel transmission setup presented in Figure 4, the WDM comb transmission channels are generated by shaping amplified spontaneous emission noise through wavelength selective switches (WSS) for each band (C and L), separately. After the generation, the channels pass by the C- and L-band Booster EDFAs and are subsequently multiplexed by a 3 dB coupler. This comb is then combined with the channel under test (CUT), generated the same way as described in Section 2. The comb consists of 20 channels in the C-band and 22 channels in the L-band, with a spacing of 150 GHz, a flat launch power profile of 14.9 dBm in total and a gap between each band of around 1.645 THz. At the receiver, the WDM comb is boosted by a C+L EDFA before passing through a bandpass filter (BPF), which selects the CUT. Before filtering, the signal is also used for signal-to-noise ratio measurements in an OSA. Finally, the signal is amplified one last time before mixing with the local oscillator (LO) in the coherent receiver.

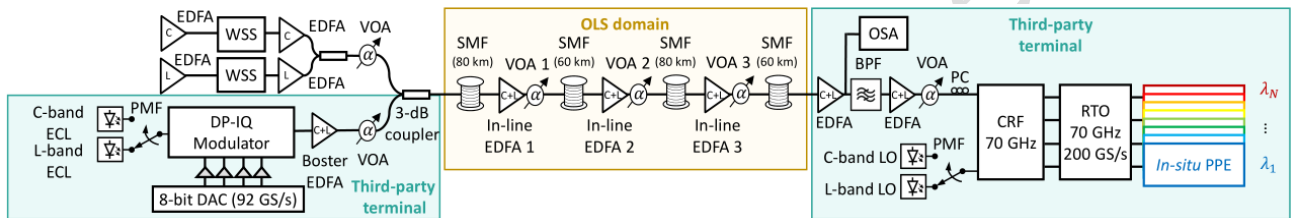


Figure 4: Experimental testbed used in the multi-channel transmission link tomography.

The first result shown in Figure 5 (a) is the estimated spectral power profile based on the link tomography applied for WDM transmission. It is worth mentioning that, for this case, unlike the case presented in Section 2, the input power experienced by each individual amplifier may vary. We also show in Figure 5 (b-e) the estimated power peaks at the input of the OLS and output of ILA's 1, 2, and 3. The gain tilt raised, mainly by WDM transmission and amplifiers characteristics, is successfully captured by the link tomography, as shown by the red markers in these plots.

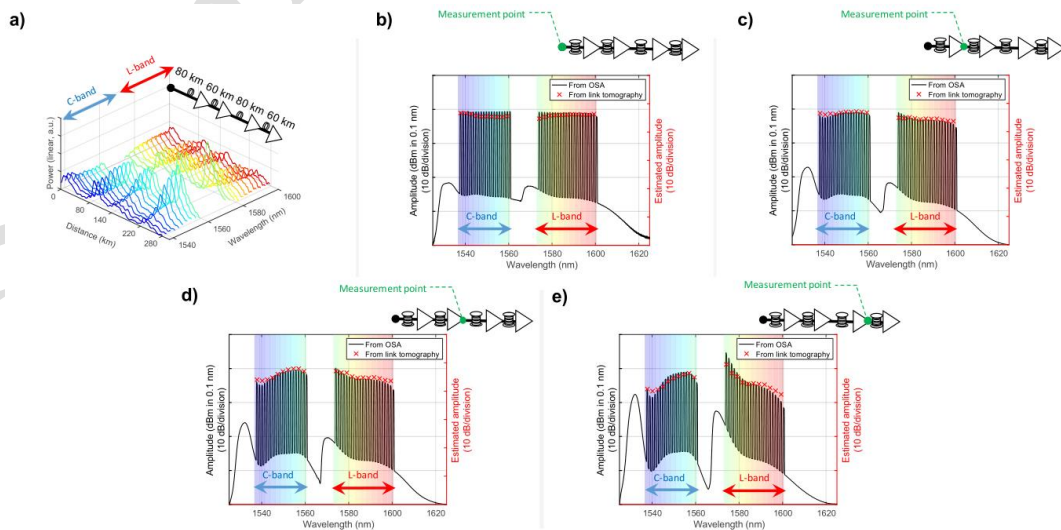


Figure 5: (a) Link tomography obtained in Experiment II (multi-channel analysis). Power peak curves obtained from the link tomography obtained at (b) input of the OLS, and output of the ILA (c) 1, (d) 2 and (e) 3 link.

Even with the link tomography being able to capture the tilt of this transmission, other factors, such as the channel-loading configurations or variations in channel input power [10], can worsen amplification tilts. To emulate this behaviour, a VOA with 6 dB of flat loss is added at the input of ILA 2. The anomaly scheme used for this case is the same as the one presented in Section 2 and shown in Figure 6 (a). By the heatmap presented in Figure 6 (b), is possible to see two anomalies. The first is the emulated tilt raised by the VOA at the ILA 2 input at around 140 km. The second observed anomaly is the cascade effect raised in the ILA 3, a consequence of the difference of input power generated by the VOA. These results attest that link tomography can be beneficial in determining wavelength-dependent disruptions in optical links.

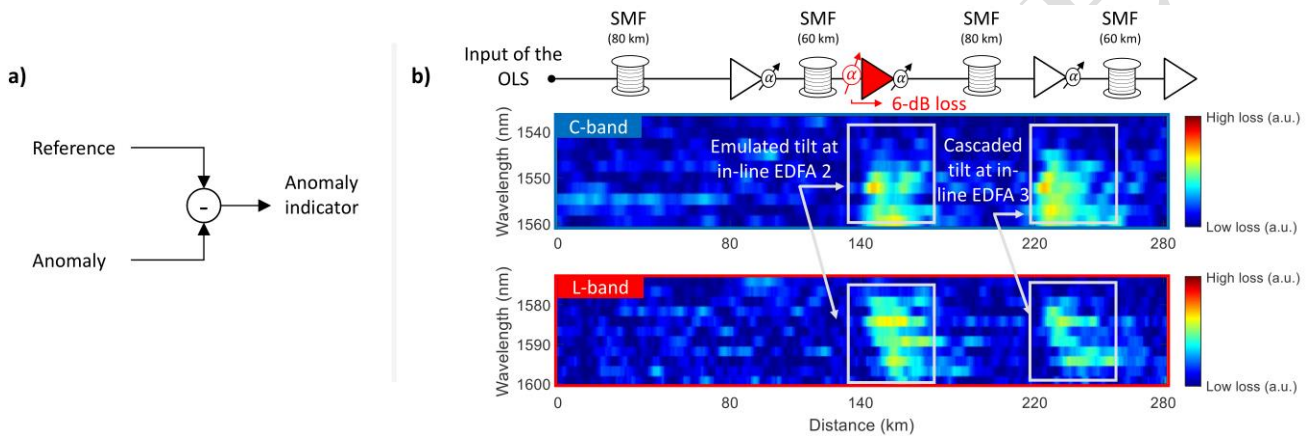


Figure 6: (a) Anomaly detection scheme based on subtraction. (b) Estimated anomaly heatmap for VOA with 6 dB of spectrally flat loss applied at the input of ILA 2.

Even with the subtraction detection scheme showing good results, a more location accurate scheme is desirable, in order to cope with the non-uniformity and sparsity of the signatures which can hinder the identification of the problem. One alternative to increase the location accuracy of detection schemes in link tomography is the insertion of a numerical differentiation with respect to the spatial domain [11], presented in

Figure 7 (a). In [9] is proposed the usage of wavelet denoising of the link tomography [10] and shown in

Figure 7 (b). This scheme is added between the subtraction and the numerical differentiation and is composed by a discrete wavelet transformation (DWT), followed by soft-threshold procedure and an inverse DWT (iDWT) before been forward to the numerical differentiation. The wavelet denoising must be able to remove the undesired noise within the signal.

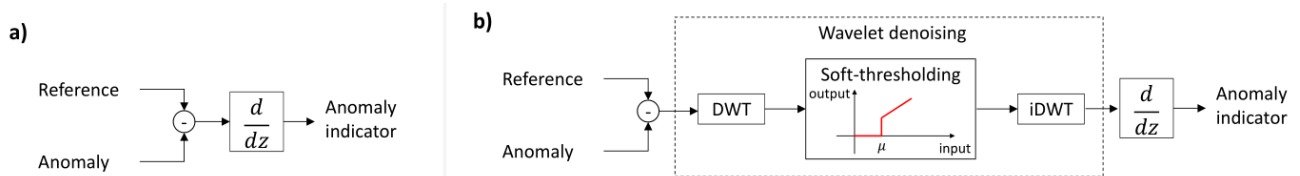


Figure 7: Anomaly detection schemes based on (a) subtraction plus numerical differentiation, and (b) wavelet denoising.

In order to evaluate the performance of these detection schemes, we emulate two anomalies in ILA's 2 and 3, installing a VOA at the output of these amplifiers with 3 dB of flat attenuation. This type of anomaly could correspond to excessive loss from amplifier-to-fiber connectors or depletion of amplifier's pump current. The heatmaps presented in

Figure 8 (a-b) for failures in ILA's 2 and 3, respectively, shown that applying only the numerical differentiation to the detection scheme can generate a rough indication of the failures, but clearly leaves a non-uniform and noise pattern in the heatmap. Alternatively, applying the wavelet denoising to the detection scheme and presented in

Figure 8 (c-d) shows that this method increases the failure uniformity on the heatmap, also reducing its noise. Moreover, as presented in

Figure 8 (e), we can see that wavelet denoising is also able to present a more accurate anomaly location.

Figure 8 (e) shows for a fixed CUT wavelength (1549 nm) the subtraction plus numerical differentiation and the proposed wavelet denoising. We can see that by using wavelength denoising, the detection scheme was able to improve the accuracy of the fault detection by 3 km. Furthermore, wavelet denoising delivers a smoother profile, which provides an easier way to detect the real anomaly peak.

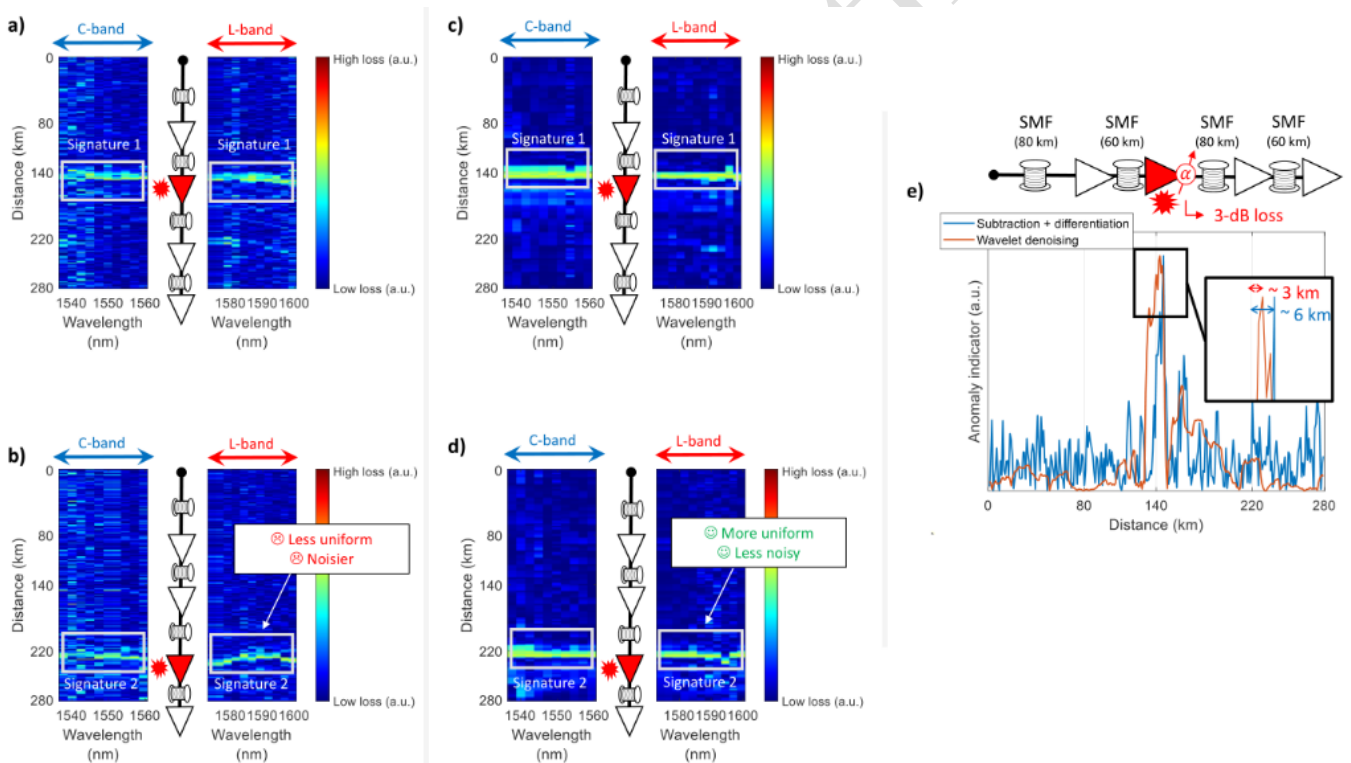


Figure 8: Estimated anomaly heatmaps for subtraction plus numerical differentiation in (a) ILA 2 and (b) ILA 3, and for wavelet denoising in (c) ILA 2 and (d) ILA 3. (e) Comparison of anomaly detection curve in EDFA 2 in wavelength 1549 nm using subtraction plus numerical differentiation and wavelet denoising.

The results presented in this section suggest that DSP link tomography can be used to accurately estimate the spectral power profile, and amplifier gain and failures for WDM multi-channel transmission without directly using measurement devices. It is also shown that the usage of wavelet denoising in anomaly detection schemes brings advantages in terms of more uniform, less noisy and more accurate results.

## 4. Conclusions

This work experimentally demonstrates a receiver-DSP scheme, which can extract the distance-wide and wavelength-dependent channel power evolution without any testing equipment or access to infrastructure information. For single-channel transmission, an estimation for the gain profile of C+L EDFAs was presented, achieving a maximum mean error of 0.6 dB. Moreover, a good level of fidelity in visualizing soft-failures such as amplifiers gain tilts is shown. For WDM multi-channel transmission, the link tomography is also able to provide an accurate power profile evolution, as well as amplifier gains and failures. Moreover, the proposed anomaly detection scheme using wavelet denoising delivered a more uniform and less noisy readings of anomaly signatures, improved the location of the fault by 3 km and delivers a smoother anomaly detection curve, providing an easier way to detect the anomalies. These results demonstrate that this approach can be used as a tool for fault detection in MBT systems.

## 5. REFERENCES

- [1] A. Napoli, N. Costa, J. K. Fischer, J. Pedro, S. Abrate, N. Calabretta, W. Forysiak, E. Pincemin, J. P.-P. Gimenez, C. Matrakidis, G. Roelkens und V. Curri, „Towards multiband optical systems,“ in *Advanced Photonics 2018 (BGPP, IPR, NP, NOMA, Sensors, Networks, SPPCom, SOF)*, 2018.
- [2] T. Tanimura, S. Yoshida, K. Tajima, S. Oda und T. Hoshida, „Concept and implementation study of advanced DSP-based fiber-longitudinal optical power profile monitoring toward optical network tomography [Invited],“ *Journal of Optical Communications and Networking*, Bd. 13, Nr. 10, pp. E132-E141, 2021.
- [3] T. Tanimura, K. Tajima, S. Yoshida, S. Oda und T. Hoshida, „Experimental demonstration of a coherent receiver that visualizes longitudinal signal power profile over multiple spans out of its incoming signal,“ in *45th European Conference on Optical Communication (ECOC 2019)*, 2019.
- [4] T. a. N. M. a. Y. E. Sasai, S. Yamamoto, H. Nishizawa und Y. Kisaka, „Digital Backpropagation for Optical Path Monitoring: Loss Profile and Passband Narrowing Estimation,“ in *2020 European Conference on Optical Communications (ECOC)*, 2020.
- [5] T. Sasai, M. Nakamura, S. Okamoto, F. Hamaoka, S. Yamamoto, E. Yamazaki, A. M. H. Nishizawa und Y. Kisaka, „Simultaneous Detection of Anomaly Points and Fiber Types in Multi-Span Transmission Links Only by Receiver-Side Digital Signal Processing,“ in *2020 Optical Fiber Communications Conference and Exhibition (OFC)*, 2020.
- [6] T. Sasai, M. Nakamura, T. Kobayashi, H. Kawakami, E. Yamazaki und Y. Kisaka, „Revealing Raman-amplified Power Profile and Raman Gain Spectra with Digital Backpropagation,“ in *2021 Optical Fiber Communications Conference and Exhibition (OFC)*, 2021.
- [7] M. Eto, K. Tajima, S. Yoshida, S. Oda und T. Hoshida, „Location-resolved PDL Monitoring with Rx-side Digital Signal Processing in Multi-span Optical Transmission System,“ in *2022 Optical Fiber Communications Conference and Exhibition (OFC)*, 2022.
- [8] M. Sena, R. Emmerich, B. Shariati, J. K. Fischer und R. Freund, „Link Tomography for Amplifier Gain Profile Estimation and Failure Detection in C+L-band Open Line Systems,“ in *2022 Optical Fiber Communications Conference and Exhibition (OFC)*, 2022.
- [9] M. Sena, P. Hazarika, C. Santos, B. Correia, R. Emmerich, B. Shariati, A. Napoli, V. Curri, W. Forysiak, C. Schubert, J. K. Fischer und R. Freund, „Advanced DSP-based Monitoring for Spatially resolved and Wavelength-dependent Amplifier Gain Estimation and Fault Location in C+L-band Systems,“ *Journal of Lightwave Technology*, pp. 1-10, 2022.
- [10] J. Yu, S. Zhu, C. L. Gutterman, G. Zussman und D. C. Kilper, „Machine-learning-based EDFA gain estimation [Invited],“ *Journal of Optical Communications and Networking*, Bd. 13, Nr. 4, pp. B83-B91, 2021.
- [11] T. Tanimura, S. Yoshida, K. Tajima, S. Oda und T. Hoshida, „Fiber-Longitudinal Anomaly Position Identification Over Multi-Span Transmission Link Out of Receiver-end Signals,“ *Journal of Lightwave Technology*, Bd. 38, Nr. 9, pp. 2726-2733, 2020.